

SPARSE POLYNOMIAL CHAOS-BASED ROBUST OPTIMIZATION DESIGN OF AERODYNAMIC AND SONIC BOOM

Shekun Wang[1] & Huan Zhao[1]

[1]School of Aeronautics, Northwestern Polytechnical University, Xi'an, Shaanxi 710072, China

Abstract

Robust aerodynamic and sonic boom design under uncertainty is an important requirement for future supersonic civil aircraft, because flight-condition and atmospheric variations can significantly affect both aerodynamic performance and perceived boom loudness. This paper develops a sparse polynomial chaos expansion (PCE)-based framework for uncertainty quantification and robust optimization with limited high-fidelity samples. The method combines non-intrusive PCE modeling with sparse coefficient identification to improve surrogate efficiency in a small-sample setting. The framework is applied to the robust design of the JAXA wing-body configuration under uncertainties in Mach number, angle of attack, Reynolds number, altitude, and humidity. The results show that the proposed approach preserves the statistical level of aerodynamic performance while reducing both the mean and the standard deviation of the sonic boom loudness metric PLdB. These results indicate that sparse PCE provides an effective and computationally affordable basis for aerodynamic/sonic boom robust design under multi-source uncertainty.

Keywords: Sonic boom; Robust optimization; Uncertainty quantification; Sparse polynomial chaos

1. Introduction

Supersonic civil transport remains attractive because it can shorten intercontinental travel time substantially. Yet the reintroduction of civil supersonic flight is still constrained by a fundamental multidisciplinary design conflict: the aircraft must simultaneously maintain favorable aerodynamic efficiency, satisfy trim and performance requirements, and suppress the ground-level sonic boom that limits routine overland operation. In practice, these objectives cannot be separated cleanly. Geometric changes introduced to weaken the near-field pressure signature generally affect lift, drag, and pitching moment, whereas operating and atmospheric variations influence both the aerodynamic state and the boom propagation process. Consequently, the design of a viable low-boom configuration is not only a deterministic shape-optimization problem, but also an optimization-under-uncertainty problem in which the statistical stability of the design is as important as its nominal performance [1, 2, 3, 4].

This issue has become more important as low-boom design methodologies have matured from nominal concept shaping toward certification-oriented performance assessment. Even when a configuration produces an acceptable boom signature at its nominal cruise point, the perceived loudness at the ground can change noticeably under perturbations in Mach number, angle of attack, Reynolds number, altitude, humidity, temperature, density, or wind-related atmospheric conditions [5, 6, 7, 8, 9]. The same perturbations also modify the aerodynamic coefficients that determine cruise efficiency and the trim state, thereby changing the trade-off between low-boom performance and aerodynamic quality. A design obtained from deterministic optimization may therefore be highly sensitive to realistic off-design conditions and may lose part of its nominal benefit when uncertainty is taken into account. For this reason, robust design optimization has become an increasingly important theme in aerospace design, where one seeks configurations with not only improved mean performance but also reduced variability and improved reliability under uncertain operating environments [3, 4, 10, 11].

The broader aerodynamic-design literature has shown that robust optimization under uncertainty is conceptually straightforward but computationally demanding. A typical formulation requires repeated evaluations of statistical objectives and constraints, often involving nested loops in which an outer optimizer proposes design changes while an inner uncertainty-propagation step estimates the moments or reliability metrics of each candidate design. For expensive CFD-based design problems, this double-loop structure can be prohibitive unless the uncertainty quantification step is made substantially more efficient [3, 4, 12, 10, 11]. This challenge is particularly severe in supersonic low-boom design, because each sample may involve geometry deformation, flow-field analysis, extraction of the near-field pressure signature, and subsequent boom loudness evaluation. As the number of uncertain variables grows, direct Monte Carlo sampling becomes unattractive, and the cost of repeated robust optimization can quickly exceed practical design budgets.

Accordingly, uncertainty quantification for sonic boom prediction and low-boom design has received increasing attention in recent years [13, 5, 6, 7, 8, 14, 9]. Walker et al. [6] investigated the propagation of pressure-signature uncertainty to ground loudness, and Jeong et al. [7] demonstrated that polynomial chaos can provide an efficient non-intrusive framework for sonic boom analysis under atmospheric uncertainty. West et al. [5] further highlighted the role of uncertainty quantification in the assessment and eventual certification of low-boom configurations. On the design side, Colonno and Alonso [1] revisited sonic boom minimization from a robustness perspective and argued that useful low-boom designs must combine favorable nominal performance with reduced sensitivity to perturbations. Makino and Kroo [2] proposed robust sonic boom objective functions, Rallabhandi et al. [9] developed an atmospheric-adjoint-based robust design strategy, and Schaefer et al. [14] recently showed the promise of polynomial-chaos-based robust design for spatially accurate sonic boom prediction. Multifidelity strategies have also been explored to reduce cost in uncertainty-aware sonic boom analysis [8, 12]. Taken together, these studies clearly establish that uncertainty-aware low-boom design is necessary and technically feasible.

However, several gaps remain between these advances and the needs of a practical robust-design framework for simultaneous aerodynamic and sonic boom optimization. First, many existing studies focus primarily on uncertainty propagation for a fixed configuration, which is valuable for analysis but does not by itself resolve the repeated many-query burden inside a robust optimizer. Second, some robust-design approaches emphasize atmospheric effects or sonic boom metrics alone, whereas a realistic design process must account for the joint response of aerodynamic performance and boom loudness under the same uncertain operating conditions. Third, even when surrogate models are introduced, their efficiency can deteriorate rapidly in mixed design-uncertainty spaces, especially when the number of available high-fidelity samples is limited relative to the growth of the approximation basis [12, 15, 16, 17]. In this setting, full polynomial-chaos regression may become unstable, while more general surrogate approaches such as Kriging still require additional sampling to estimate moments. What is needed is a surrogate that remains tractable in moderate-to-high stochastic dimension, can be trained from limited samples, and allows the statistical quantities required by robust optimization to be evaluated directly and efficiently.

Polynomial chaos expansion (PCE) is a natural candidate because it provides a spectral representation of the response with respect to uncertain inputs and enables direct extraction of moments from the expansion coefficients [18, 19]. Non-intrusive variants have been applied successfully in aerodynamic and sonic boom uncertainty analysis [13, 7], and data-driven generalizations such as arbitrary polynomial chaos further broaden the applicability of the approach when input distributions are not restricted to classical canonical forms [20]. More generally, the uncertainty-quantification literature now contains a substantial body of work showing that sparse PCE should be viewed as a family of sample-efficient surrogate constructions whose performance depends on basis truncation, regression strategy, and experimental design [21, 22, 17]. This broader perspective is useful for positioning the present work, but the objective here is not to develop a new sparse-regression algorithm. Instead, the practical question is which non-intrusive surrogate remains sufficiently accurate and efficient in the small-sample, multi-parameter regime relevant to expensive aerodynamic and sonic boom analysis. For this reason, the present paper deliberately restricts attention to least-angle-regression-based sparse PCE, together with full regression PCE, Kriging, and direct Monte Carlo as comparison base-

lines. Within that restricted scope, sparse identification remains attractive because it suppresses the ill-conditioning associated with oversized polynomial bases while preserving direct access to the response moments required by robust optimization [23, 21].

Against this background, the present paper develops a sparse PCE-based robust optimization framework for aerodynamic and sonic boom design under multi-source uncertainty. The framework is intended for situations in which high-fidelity samples are expensive, the uncertain space contains several operating and atmospheric parameters, and the designer is concerned with both nominal trends and variability. Five uncertain parameters are considered in the present study, namely Mach number, angle of attack, Reynolds number, flight altitude, and atmospheric humidity. A sparse polynomial-chaos surrogate is constructed to represent the responses of aerodynamic quantities and sonic boom loudness, and the resulting surrogate is embedded in a robust optimization loop for the JAXA wing-body configuration. Because the final optimization depends directly on statistical moments, the paper also includes a benchmark comparison against full regression PCE, Kriging, and direct Monte Carlo estimation in order to justify the selected uncertainty-propagation model before applying it to the aerodynamic/sonic boom design problem.

The main contributions of the paper are threefold. First, a limited-sample benchmark study is carried out to assess the relative suitability of full PCE, LARS-PCE, Kriging, and direct Monte Carlo for mean and standard-deviation estimation in problems of increasing dimensionality. Second, a sparse-PCE-based robust optimization formulation is built for simultaneous control of aerodynamic statistics and sonic boom statistics under five uncertain operating parameters. Third, the resulting framework is demonstrated on the JAXA wing-body configuration, where the optimized design preserves the statistical level of aerodynamic performance while reducing both the mean and the standard deviation of the sonic boom loudness metric. In this sense, the work is aimed not merely at improving nominal low-boom performance, but at producing designs whose acoustic and aerodynamic behavior is more reliable in realistic flight environments.

The remainder of the paper is organized as follows. Section 2 summarizes the sparse PCE formulation used in this work. Section 3 compares several uncertainty-propagation strategies on benchmark functions and explains the selection of the surrogate model used later in robust optimization. Section 4 describes the robust optimization framework and the numerical setup. Section 5 presents and discusses the optimization results. Section 6 concludes the paper.

2. Sparse Polynomial Chaos Surrogate Modeling

2.1 Polynomial Chaos Representation of the Response

The role of polynomial chaos expansion (PCE) in the present work is to provide a surrogate model for repeated uncertainty propagation inside the optimization loop. Rather than treating PCE as a standalone uncertainty-quantification exercise, it is used here as an intermediate model between expensive aerodynamic/sonic boom simulations and the statistical objectives required by robust optimization.

Let

$$\mathbf{X} = (x_1, x_2, \ldots, x_M) \in \mathbb{R}^M \tag{1}$$

denote the uncertain-input vector and let

$$Y = \mathscr{M}(\mathbf{X}) \tag{2}$$

be a scalar model response of interest, where $\mathscr{M}(\cdot)$ is the deterministic analysis operator. In the present study, the uncertain inputs represent operating and atmospheric variables, while the responses include aerodynamic coefficients and the sonic boom loudness metric. Assuming that $Y \in L^2$, the response admits a polynomial-chaos expansion in a basis associated with the probability measure of $\mathbf{X}$ [18]:

$$Y = \sum_{j=0}^{\infty} \beta_j \Psi_j(\mathbf{X}). \tag{3}$$

When the components of $\mathbf{X}$ are mutually independent, the joint density can be factorized as

$$f_{\mathbf{X}}(\mathbf{x}) = \prod_{i=1}^{M} f_{x_i}(x_i), \tag{4}$$

and the multivariate basis functions are constructed as tensor products of one-dimensional orthonormal polynomials,

$$\Psi_j(\mathbf{X}) = \prod_{i=1}^{M} \phi^{(i)}_{\alpha_i^{(j)}}(x_i), \qquad \mathbb{E}[\Psi_i(\mathbf{X})\Psi_j(\mathbf{X})] = \delta_{ij}, \tag{5}$$

where $\alpha^{(j)} = (\alpha_1^{(j)}, \ldots, \alpha_M^{(j)})$ is the multi-index associated with the j-th basis term and δ_{ij} is the Kronecker delta. The corresponding coefficients β_j measure the contribution of each basis function to the stochastic response.

In practical computation, the infinite expansion is truncated to a finite admissible index set $\mathscr{A}$, yielding

$$Y \approx \widehat{Y} = \sum_{\alpha \in \mathscr{A}} \beta_\alpha \Psi_\alpha(\mathbf{X}) + \varepsilon(\mathbf{X}), \tag{6}$$

where $\varepsilon(\mathbf{X})$ denotes the truncation error. For a total-order truncation of degree n in an M-dimensional stochastic space, the number of candidate basis terms is

$$p = |\mathscr{A}| = \binom{M+n}{n}. \tag{7}$$

In the present application, this truncation step is essential because the number of candidate terms grows rapidly once both design variables and uncertain variables are considered together.

The orthonormality of the basis gives PCE a particularly useful property for robust optimization: the low-order moments of the surrogate can be recovered directly from the coefficients. Specifically,

$$\mu_Y = \mathbb{E}[\widehat{Y}] = \beta_{\mathbf{0}}, \tag{8}$$

and

$$\sigma_Y^2 = \mathrm{Var}[\widehat{Y}] = \sum_{\alpha \in \mathscr{A} \setminus \{\mathbf{0}\}} \beta_\alpha^2. \tag{9}$$

This direct moment-evaluation property is one of the main reasons why PCE is attractive for statistical design optimization: once the surrogate has been identified, repeated estimation of means and standard deviations no longer requires additional Monte Carlo sampling.

The choice of one-dimensional orthogonal polynomial family is determined by the probability distribution of each input variable. Common correspondences between random variable distributions and their associated orthogonal polynomials are summarized in Table 1.

Table 1 – Orthogonal polynomial and the corresponding type of random input variable.

Random variable distribution	Orthogonal polynomial type	Support
Gaussian	Hermite	$(-\infty, +\infty)$
Uniform	Legendre	$[a, b]$
Gamma	Laguerre	$[0, +\infty)$
Poisson	Charlier	$\{0, 1, 2, \ldots\}$
Beta	Jacobi	$[a, b]$

2.2 Sparse Identification and Surrogate Construction

For the robust optimization problem considered here, the candidate basis is built in a space that contains both geometric variables and uncertain operating variables. As a result, the full truncated basis can become much larger than the number of available high-fidelity samples. Under these circumstances, a full least-squares regression is inefficient and can easily become ill-conditioned. A sparse approximation is therefore adopted so that only the most influential polynomial terms are retained.

Consider an experimental design

$$\mathscr{D} = \{\mathbf{x}^{(i)}, y^{(i)}\}_{i=1}^{N}, \qquad y^{(i)} = \mathscr{M}(\mathbf{x}^{(i)}), \tag{10}$$

and define the information matrix

$$\Psi_{ij} = \Psi_j(\mathbf{x}^{(i)}), \tag{11}$$

with response vector $\mathbf{Y} = [y^{(1)}, \ldots, y^{(N)}]^T$. If all candidate basis terms are retained, the non-intrusive coefficient estimation problem may be written as

$$\widehat{\beta}_{\mathrm{LS}} = \arg\min_{\beta} \|\mathbf{Y} - \Psi\beta\|_2^2. \tag{12}$$

This formulation is adequate only when the experimental design is sufficiently rich relative to the candidate basis size. In the mixed design-uncertainty setting of the present work, however, the ratio between the number of samples and the number of basis terms can become unfavorable, and the full regression problem may then produce unstable or overfitted surrogates.

The sparse identification problem can be formulated as the search for the smallest active basis that reproduces the sampled response with acceptable error:

$$\min_{\beta} \|\beta\|_0 \quad \text{s.t.} \quad \|\mathbf{Y} - \Psi\beta\|_2 \leq \varepsilon, \tag{13}$$

where $\|\beta\|_0$ denotes the number of non-zero coefficients and ε is a prescribed approximation tolerance. Because direct ℓ_0-minimization is NP-hard, it is commonly relaxed to an ℓ_1-regularized or LASSO-type problem,

$$\widehat{\beta} = \arg\min_{\beta} \left(\|\mathbf{Y} - \Psi\beta\|_2^2 + \lambda \|\beta\|_1 \right), \tag{14}$$

which provides a practical route to sparse reconstruction and is closely related to compressive-sensing ideas. In robust design applications, this sparse treatment is particularly useful because the dominant stochastic trends are often governed by a relatively small subset of basis terms even when the nominal candidate basis is large.

Among practical sparse-identification algorithms, least angle regression (LAR) and its LASSO-related variants [23] have been widely adopted for sparse PCE construction. Blatman and Sudret [21] showed that LAR-based sparse PCE can identify compact and accurate surrogate models with substantially fewer samples than a full regression-based expansion. The algorithm builds a sequence of nested active sets by adding the basis term that is most correlated with the current residual and recomputing the regression on the active set. The final surrogate is then selected from this path by an error indicator such as a corrected leave-one-out estimate of the generalization error [21]. In this way, the procedure balances approximation richness against overfitting without requiring an exhaustive search over all possible subsets.

After sparse identification, the response is represented as

$$\widehat{Y}(\mathbf{X}) = \beta_{\mathbf{0}} + \sum_{\alpha \in \mathscr{A}^*} \beta_\alpha \Psi_\alpha(\mathbf{X}), \tag{15}$$

where $\mathscr{A}^* \subseteq \mathscr{A}$ is the selected active basis. For the purposes of the present paper, the key point is that sparse PCE provides a tractable approximation of the response surface in a mixed design-uncertainty space while preserving direct access to the moments required by robust optimization. Once this approximation is available, quantities such as means and standard deviations can be evaluated much more efficiently than by repeated direct high-fidelity simulation. This property is what makes LARS-PCE attractive for robust aerodynamic and sonic boom optimization.

3. Benchmark Comparison of Uncertainty-Propagation Methods

Before embedding a surrogate model into the robust aerodynamic/sonic boom optimization loop, it is necessary to determine which uncertainty-propagation strategy provides the best compromise between accuracy and computational efficiency in a limited-sample setting. Four representative benchmark problems are therefore considered: the three-dimensional Ishigami function, the six-dimensional OTL circuit, the eight-dimensional Borehole function, and the ten-dimensional Wing weight function. These cases cover different levels of nonlinearity and dimensionality while remaining standard test functions in the uncertainty-quantification literature. Their model forms are summarized

Table 2 – Benchmark models used in the uncertainty-propagation study.

Case	Dim	Model form
Ishigami	3	$y = \sin x_1 + 7\sin^2 x_2 + 0.1x_3^4 \sin x_1$
OTL circuit	6	$V_{b1} = 12R_{b2}/(R_{b1}+R_{b2})$, $y = \frac{(V_{b1}+0.74)\beta(R_{c2}+9)}{\beta(R_{c2}+9)+R_f} + \frac{11.35R_f}{\beta(R_{c2}+9)+R_f} + \frac{0.74R_f\beta(R_{c2}+9)}{[\beta(R_{c2}+9)+R_f]R_{c1}}$
Borehole	8	$y = \frac{2\pi T_u(H_u - H_l)}{\ln(r/r_w)\left[1 + \frac{2LT_u}{\ln(r/r_w)r_w^2 K_w} + \frac{T_u}{T_l}\right]}$
Wing weight	10	$y = 0.036S_w^{0.758}W_{fw}^{0.0035}A^{0.6}(\cos\Lambda)^{-1.2}q^{0.006}\lambda^{0.04}(100t_c)^{-0.3}(N_zW_{dg})^{0.49} + S_wW_p$

in Table 2, while the corresponding input distributions and PCE settings are listed in Table 3. For Ishigami, the true mean and standard deviation are known analytically; for the other three cases, the reference values are obtained from Sobol-sequence Monte Carlo estimation with 2×10^5 samples.

Four methods are compared on all benchmark cases: full regression PCE, sparse PCE identified by least angle regression (denoted here as LARS-PCE), Kriging followed by surrogate-based sampling for moment evaluation, and direct Monte Carlo estimation from the same training samples. For each sample size, 50 repeated experiments are performed, and the relative errors of the estimated mean and standard deviation are recorded. The comparison focuses on statistical quantities because they are the quantities required directly by the subsequent robust optimization formulation.

Figures 1, 2, 3, and 4 summarize the benchmark results. Several common trends can be observed. First, the full PCE model is consistently the least reliable choice in the limited-sample regime. Its candidate basis grows rapidly with dimension, and the resulting regression becomes unstable before enough samples are available. This behavior is visible in all four cases, where the full PCE error level remains much higher than the alternatives over a broad range of training sizes. Second, direct Monte Carlo estimation improves steadily with sample size, but its convergence is relatively slow because it does not exploit any surrogate structure. Third, Kriging often provides competitive mean estimates, especially on the smoother engineering-type responses, but the statistical moments must still be obtained through additional surrogate sampling rather than directly from the model coefficients.

By contrast, LARS-PCE shows the most favorable overall behavior. In the Ishigami case, once the sample size becomes moderate, the mean and standard deviation errors drop much faster than those of the competing methods. In the Borehole, Wing weight, and OTL circuit cases, LARS-PCE again provides the lowest or near-lowest error across most sample sizes and remains especially effective for standard-deviation estimation. Across all 62 sample-size and metric comparisons in the four benchmark cases, LARS-PCE yields the smallest median error 45 times, whereas Kriging is best 14 times, direct Monte Carlo 3 times, and full PCE never ranks first. This result indicates that sparse identification is essential once the polynomial basis becomes significantly larger than the available design of experiments.

The benchmark study also clarifies the practical reason for selecting LARS-PCE in the later robust optimization. Full PCE is too sensitive to basis growth, and direct Monte Carlo is too expensive when repeated statistical evaluation is required inside an optimizer. Kriging can be accurate, but its moments are not available in closed form and therefore require extra sampling on top of surrogate construction. LARS-PCE combines the main advantages needed in the present work: stable accuracy in limited-sample conditions, direct evaluation of the response moments from the surrogate coefficients, and a sparse representation that remains tractable in the mixed design-uncertainty space. For these reasons, the robust optimization framework developed in the following sections adopts LARS-PCE as the uncertainty-propagation model.

Table 3 – Input distributions and PCE settings for the benchmark study.

Case	Random inputs	Deg.	q	Sample sizes
Ishigami	$x_1, x_2, x_3 \sim U[-\pi, \pi]$	14	0.9	30–400
OTL circuit	$R_{b1} \sim U[50, 150]$, $R_{b2} \sim U[25, 70]$, $R_f \sim U[0.5, 3.0]$, $R_{c1} \sim U[1.2, 2.5]$, $R_{c2} \sim U[0.25, 1.2]$, $\beta \sim U[50, 300]$	6	0.9	30–500
Borehole	$r_w \sim \mathcal{N}(0.1, 0.016^2)$, $r \sim \mathcal{LN}(7.71, 1.01)$, $T_u \sim U[63070, 115600]$, $H_u \sim U[990, 1110]$, $T_l \sim U[63.1, 116]$, $H_l \sim U[700, 820]$, $L \sim U[1120, 1680]$, $K_w \sim U[9855, 12045]$	6	0.9	50–600
Wing weight	$S_w \sim U[150, 200]$, $W_{fw} \sim U[220, 300]$, $A \sim U[6, 10]$, $\Lambda \sim U[-10, 10]$, $q \sim U[16, 45]$, $\lambda \sim U[0.5, 1.0]$, $t_c \sim U[0.08, 0.18]$, $N_z \sim U[2.5, 6.0]$, $W_{dg} \sim U[1700, 2500]$, $W_p \sim U[0.025, 0.08]$	5	0.9	50–600

Each sample size is repeated 50 times using random Latin-hypercube training sets. The same hyperbolic truncation index $q = 0.9$ is used in both full PCE and LARS-PCE.

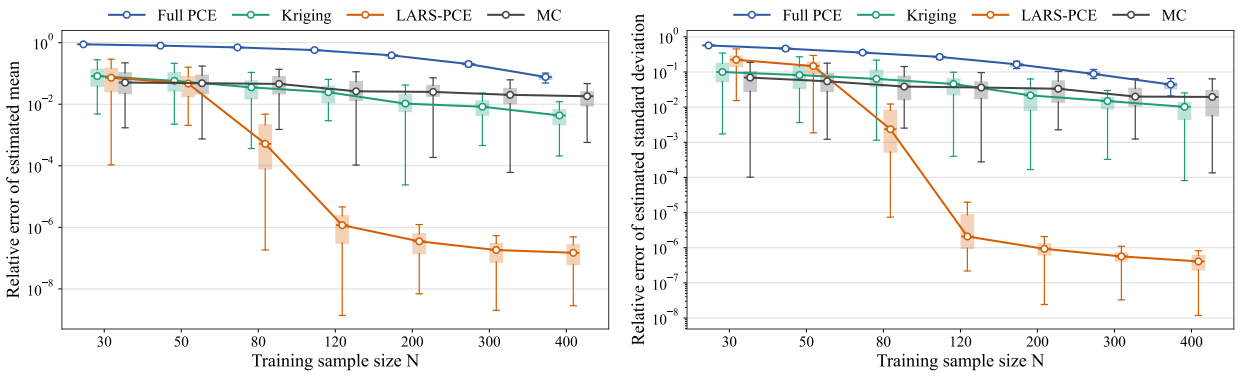


Figure 1 – Benchmark comparison for the Ishigami function: relative errors of mean and standard-deviation estimation for full PCE, LARS-PCE, Kriging, and Monte Carlo.

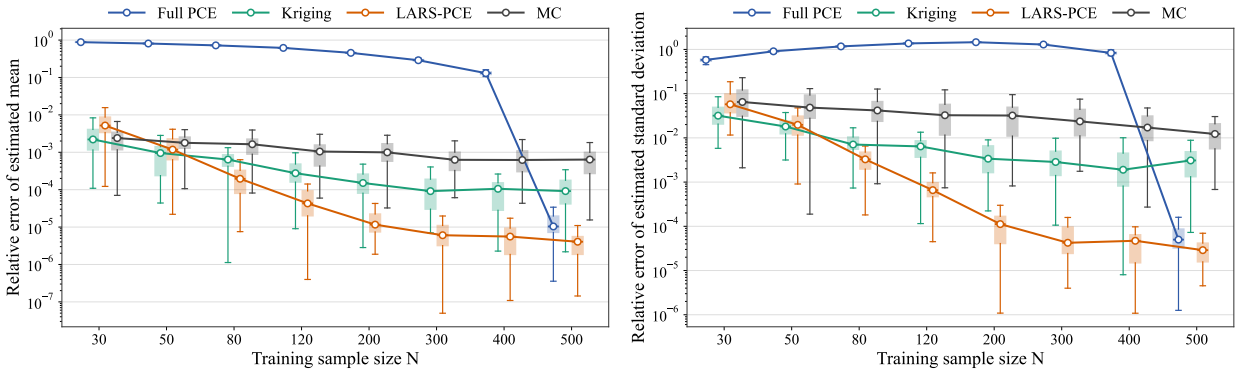


Figure 2 – Benchmark comparison for the OTL circuit: relative errors of mean and standard-deviation estimation for full PCE, LARS-PCE, Kriging, and Monte Carlo.

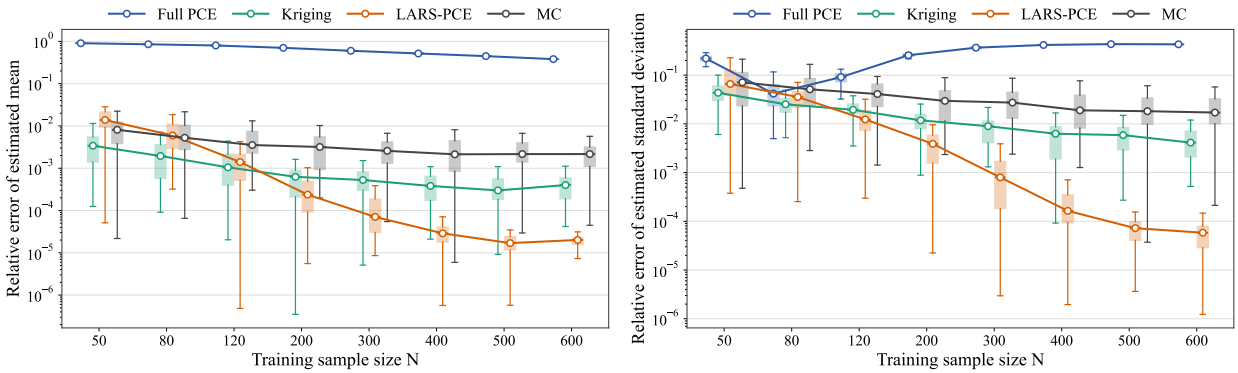


Figure 3 – Benchmark comparison for the Borehole function: relative errors of mean and standard-deviation estimation for full PCE, LARS-PCE, Kriging, and Monte Carlo.

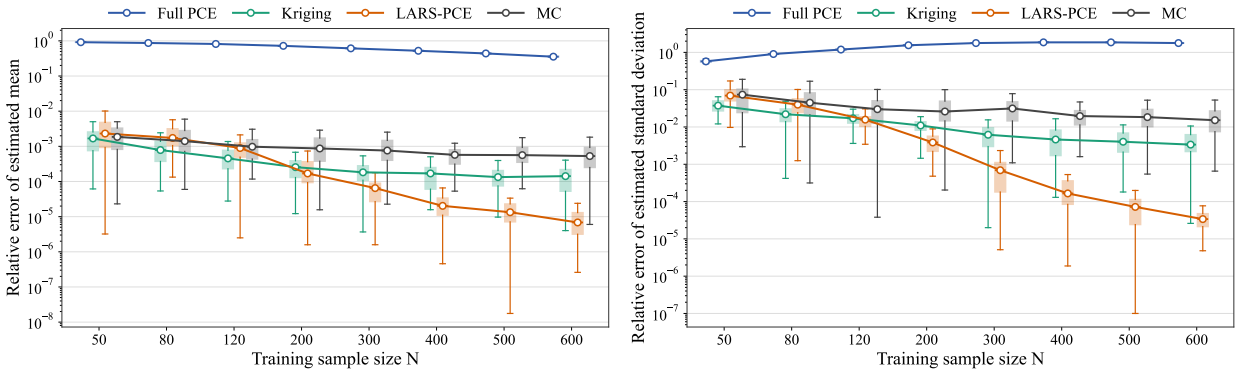


Figure 4 – Benchmark comparison for the Wing weight function: relative errors of mean and standard-deviation estimation for full PCE, LARS-PCE, Kriging, and Monte Carlo.

4. Robust Optimization Framework and Numerical Setup

4.1 Configuration and Performance Metrics

The test case considered in this study is the JAXA Wing Body (JWB) configuration provided in the Second Sonic Boom Prediction Workshop (SBPW2). This model is adopted because it is a representative low-boom configuration with a well-defined operating condition and geometric parameterization. The CFD and sonic boom calculations are performed on half-models under the baseline condition listed in Table 4.

The aerodynamic design problem considers the principal performance quantities of lift, drag, and pitching moment. For sonic boom evaluation, the perceived loudness metric PLdB is adopted. PLdB

Table 4 – CFD simulation parameter settings.

Mach number	Alpha	Body length	Reference area	Altitude	Temperature	Reynolds Number
1.6	2.3067°	$38.7\,m$	$32.8\,m^2$	$15760\,m$	$216.65\,K$	$5.7E6$

was originally introduced by Stevens [24] and later adapted by Shepherd and Sullivan [25] for low-frequency impulse-noise assessment. Because it correlates reasonably well with human perception of boom loudness, it remains a standard metric in sonic boom studies.

4.2 Problem Formulation

Five uncertain operating parameters are considered in the present robust design problem: Mach number Ma, angle of attack α, Reynolds number Re, flight altitude H, and atmospheric humidity h. These parameters are selected because they directly affect both the aerodynamic state and the sonic boom propagation environment. The optimization is therefore formulated in terms of statistical moments rather than deterministic responses.

Let $\mathbf{d}$ denote the vector of geometric design variables. The optimization seeks a design that maintains aerodynamic performance while reducing both the mean and the variability of sonic boom loudness. The statistical optimization problem considered in this study can be written as

$$
\begin{aligned}
\text{Given:} \quad & Re \in N(5.7\times10^6, (1\times10^4)^2) \\
& Ma \in N(1.6, 0.01^2) \\
& \alpha \in N(2.3067, 0.1^2) \\
& H \in N(15760, 50^2) \\
& h \in N(70, 3^2) \\
\text{Find:} \quad & \mathbf{d} \in \mathbb{R}^n \\
\text{Minimize:} \quad & \begin{cases} -\mu_{C_l}(\mathbf{d}) \\ \sigma_{C_l}(\mathbf{d}) \\ \mu_{C_d}(\mathbf{d}) \\ \mu_{PLdB}(\mathbf{d}) \\ \sigma_{PLdB}(\mathbf{d}) \end{cases} \\
\text{Subject to:} \quad & Thick(\mathbf{d}) \geq T_0
\end{aligned}
\tag{16}
$$

where μ and σ denote the mean and standard deviation under the prescribed uncertainty distributions. The formulation emphasizes two design goals: preserving aerodynamic efficiency and reducing the average level and dispersion of the sonic boom response. The thickness constraint ensures geometric feasibility during shape deformation.

4.3 Surrogate-Assisted Optimization Procedure

The overall workflow is shown in Figure 5. First, the geometric design space and uncertainty space are defined. Second, an initial database of training samples is generated for the expensive aerodynamic and sonic boom evaluations. Third, sparse PCE surrogate models are constructed for the quantities required by the robust objective. Finally, the statistical objectives and constraints are evaluated repeatedly through the surrogate models rather than through direct high-fidelity simulations. In the present implementation, the surrogate-based search is performed by particle swarm optimization (PSO). Newly selected candidate designs are then re-evaluated with the high-fidelity CFD and sonic boom analyses, appended to the database as new samples, and used to reconstruct the sparse PCE surrogates around the evolving optimum.

In practical implementation, the workflow is governed by a compromise between model fidelity and sampling cost. The aerodynamic and boom analyses provide the reference data, but the robust objective cannot be evaluated directly at every design iteration because each high-fidelity evaluation is expensive. The sparse PCE model therefore acts as an intermediate statistical model: it is trained

on a finite set of sampled responses and then used to estimate the statistical moments needed by the optimizer. The quality of the resulting robust design depends on two linked requirements: the training data must capture the dominant uncertainty-induced response variation, and the sparse identification procedure must retain the most influential polynomial terms without overfitting the limited dataset. The numerical procedure may therefore be summarized in four steps: generation of training samples in the combined design-uncertainty space, construction of sparse PCE surrogates for C_l, C_d, and PLdB, PSO-based search on the current surrogate model, and iterative database enrichment in which newly computed high-fidelity design points are added to the training set. This organization is particularly useful when the number of uncertain inputs is too large for direct repeated Monte Carlo evaluation but still moderate enough for sparse polynomial-chaos approximation.

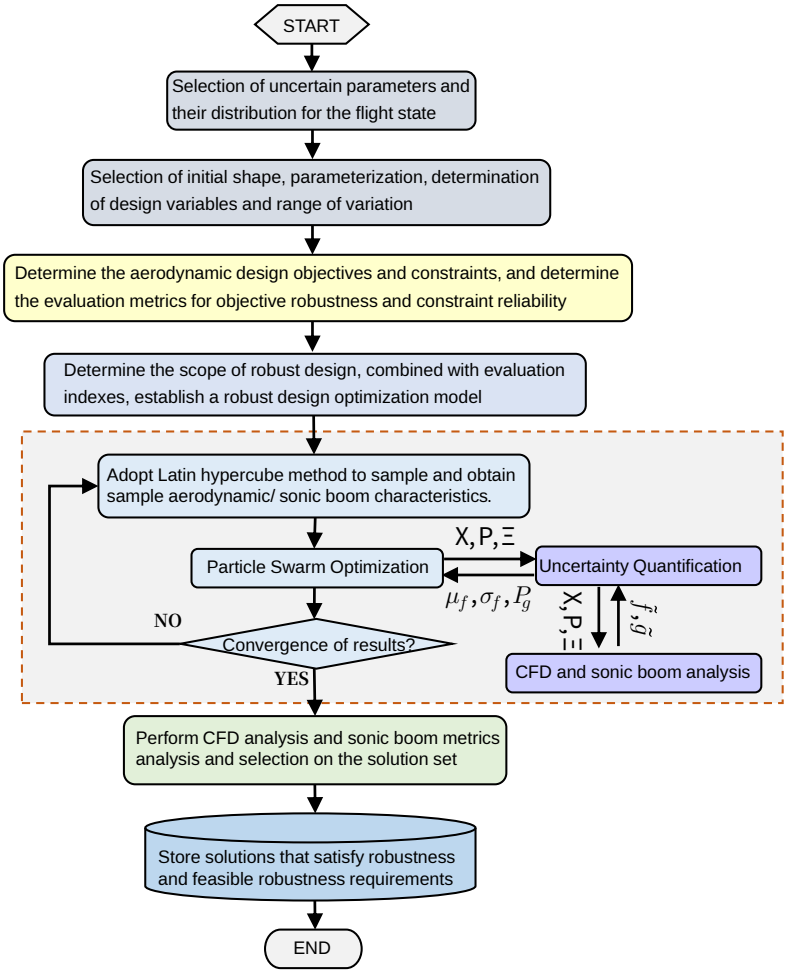


Figure 5 – Aerodynamic/sonic boom robust optimization workflow.

Shape deformation is performed using an FFD method based on multiple control frames. Eighteen wing control points are used and divided into three spanwise segments from the inner wing to the outer wing. For each segment, three control points are placed on both the upper and lower surfaces, and their motion is prescribed in the z-direction. This parameterization provides sufficient flexibility to alter the local wing thickness and camber distribution while preserving the overall planform. In the present study, the geometric variation is therefore described directly through the prescribed FFD control-point motions, without introducing additional software details into the optimization description. Figure 6 shows the distribution of the FFD control points on the JWB configuration. The control points are arranged in three spanwise groups so that the thickness and local section shape can be adjusted at representative inner-, mid-, and outer-wing locations. This arrangement is sufficient for the present study, whose purpose is not to explore an extremely high-dimensional design space, but to examine whether the robust optimization can exploit moderate geometric freedom to reduce boom sensitivity.

The surrogate should therefore be viewed not merely as a cheap regression model, but as a statistical approximation that preserves the ordering and sensitivity trends of the robust-design objectives. This feature is essential in the present application, because the optimization is driven by changes in mean values and standard deviations rather than by isolated deterministic responses.

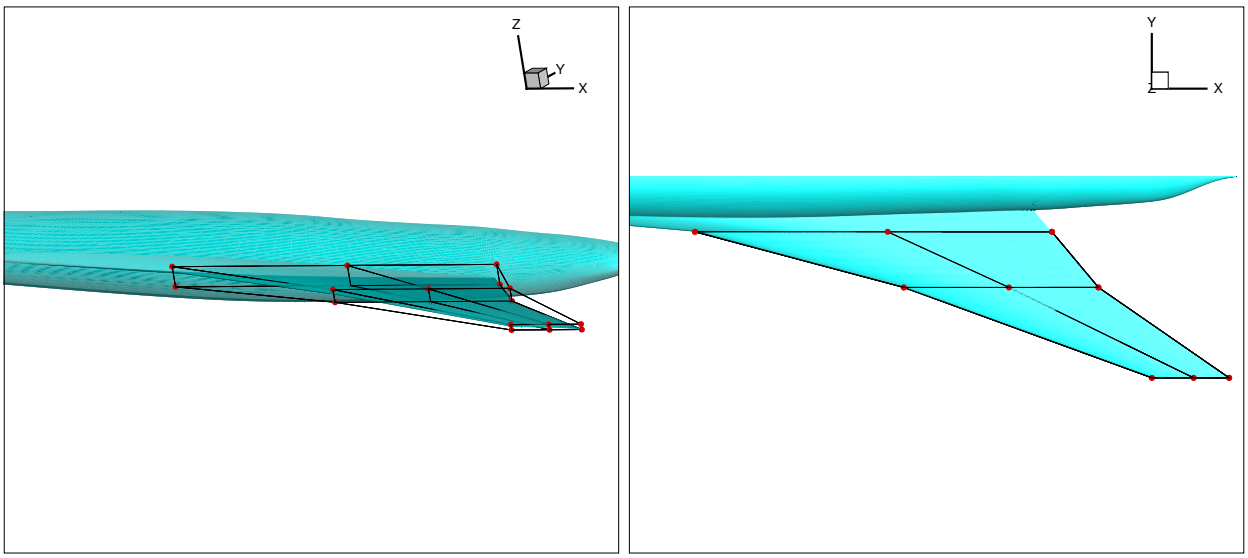


Figure 6 – Locations of the FFD control points on the JWB configuration.

4.4 Mesh and Analysis Tools

The aerodynamic analysis is carried out with the open-source SU2 solver [26]. The computational mesh is organized into three regions to balance near-body resolution and far-field efficiency. A dense near-body region encloses the half-model aircraft within a semi-cylindrical neighborhood and uses an unstructured mesh to capture the geometric detail of the configuration. Downstream of this region, the mesh is stretched along the Mach-angle direction in a structured block to improve the resolution of the propagated disturbances. The outermost region is a spherical far-field domain represented by an unstructured mesh and provides the external boundary for the aerodynamic computation.
Figure 7 illustrates both the local mesh resolution near the aircraft and the overall organization of the full computational domain. The combined mesh design reflects the dual requirement of the present problem: the near-body flow must be resolved accurately enough to extract the pressure information required for sonic boom analysis, while the outer region must remain large enough to support a stable aerodynamic solution at acceptable computational cost.

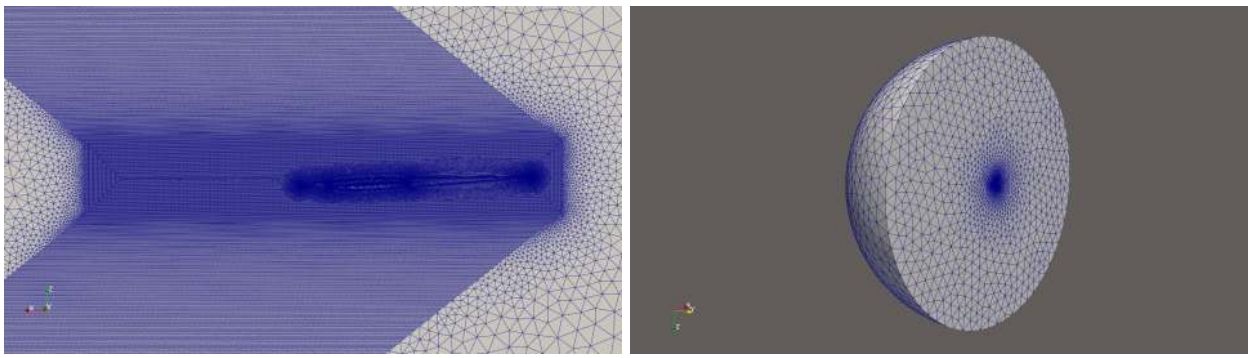


Figure 7 – Computational mesh used for the aerodynamic and sonic boom analyses: local resolution near the aircraft and overall domain layout.

5. Results and Discussion

5.1 Statistical Performance of the Optimized Design

Figure 8 compares the sample distributions of C_l, C_d, and PLdB before and after robust optimization, while Table 5 summarizes the corresponding mean values and standard deviations. Taken together, the figure and the table show that the optimized design changes the boom-related response much more strongly than the integrated aerodynamic coefficients.

For aerodynamic performance, the probability distributions of C_l and C_d remain highly overlapped between the baseline and optimized configurations. The mean of C_l changes only from 0.07315 to 0.07364, while the standard deviation changes from 0.00261 to 0.00262. Similarly, the mean of C_d decreases slightly from 0.01178 to 0.01176 and the standard deviation remains 0.00017. These small differences indicate that, under the prescribed parametric uncertainties, the robust optimization has only a limited influence on the statistical level of lift and drag. In other words, the optimization does not achieve boom reduction through a significant deterioration of the aerodynamic force coefficients.

The boom-loudness metric exhibits a substantially different behavior. As shown in Figure 8, the optimized PLdB distribution shifts toward lower values and becomes noticeably narrower. Table 5 confirms this trend: the mean PLdB decreases from 83.48035 to 82.37783, and the standard deviation decreases from 1.25764 to 0.67727. This result shows that the optimized design lowers both the expected sonic boom loudness and its sensitivity to uncertainty. From a robust-design perspective, this is the key outcome of the optimization, because it indicates simultaneous improvement in nominal performance and uncertainty tolerance.

These statistical trends are important for interpreting the design trade-off. If sonic boom reduction were accompanied by a major degradation of lift or drag performance, the resulting design would be of limited practical interest. Instead, the present results suggest a more favorable compromise: the optimized geometry retains almost the same statistical aerodynamic behavior while producing a quieter and less variable boom response. This distinction is precisely what motivates the use of uncertainty-aware optimization rather than deterministic low-boom optimization alone.

5.2 Modification of the Pressure Signature

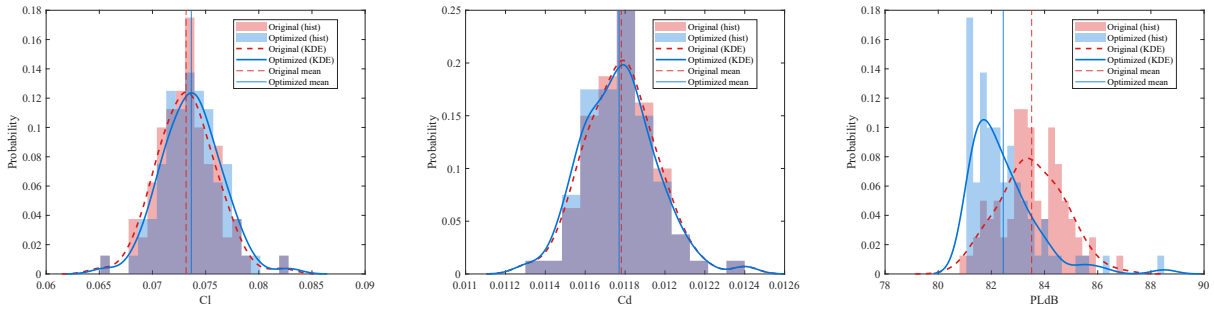
To understand the origin of the PLdB improvement, it is necessary to examine how the optimization alters the pressure signature from the near field to the ground. Figure 9 shows the streamwise distributions of the mean and standard deviation of the near-field pressure perturbation. Relative to the baseline configuration, the optimized design reduces the peak magnitudes of the mean profile in the shock-wave- and expansion-wave-related regions. At the same time, the standard deviation profile shows smaller sharp peaks near the primary shock-formation and wave-coalescence region, together with a contraction of the high-variance zone. These features indicate that the optimized geometry does not merely shift the pressure field in a deterministic sense; it also reduces the sensitivity of the near-field pressure evolution to uncertain operating conditions.

The same tendency is reflected in the ground signature shown in Figure 10. The mean ground waveform of the optimized configuration differs most clearly around the expansion-wave region, where the recovery is delayed and the minimum pressure becomes lower. More importantly, the standard deviation profile exhibits a reduction in the dominant peak associated with the major boom event, even though the full signal does not decrease uniformly at every time location. This means that the robust optimization suppresses the variability of the waveform features that contribute most strongly to perceived loudness, rather than applying a uniform reduction to the entire signal.

Taken together, the near-field and ground-signature results provide a consistent physical interpretation of the PLdB statistics. The optimized design appears to act selectively on the wave-producing pressure structure: it weakens the dominant pressure features and at the same time stabilizes them against uncertainty. This interpretation also explains why the boom-related metrics improve much more than the force coefficients. The selected design changes primarily influence the pressure-distribution details that control wave formation and propagation, while leaving the global aerodynamic balance largely unchanged.

From a broader design viewpoint, this behavior is exactly what is desired in robust low-boom optimization. A deterministic improvement in nominal PLdB alone would not guarantee a reduction in variability, whereas the present formulation explicitly targets both the mean and the standard deviation of the

response. The optimized configuration therefore achieves a more useful form of improvement: it is quieter on average and less sensitive to uncertain conditions. At the same time, the present conclusions remain tied to the current uncertainty set, geometric parameterization, and surrogate-assisted framework. Further assessment on broader design spaces and alternative uncertainty definitions would be valuable in future work.



(a) (b) (c)

Figure 8 – Probability distributions of the lift coefficient C_l, drag coefficient C_d, and perceived sonic boom level PLdB before and after robust optimization.

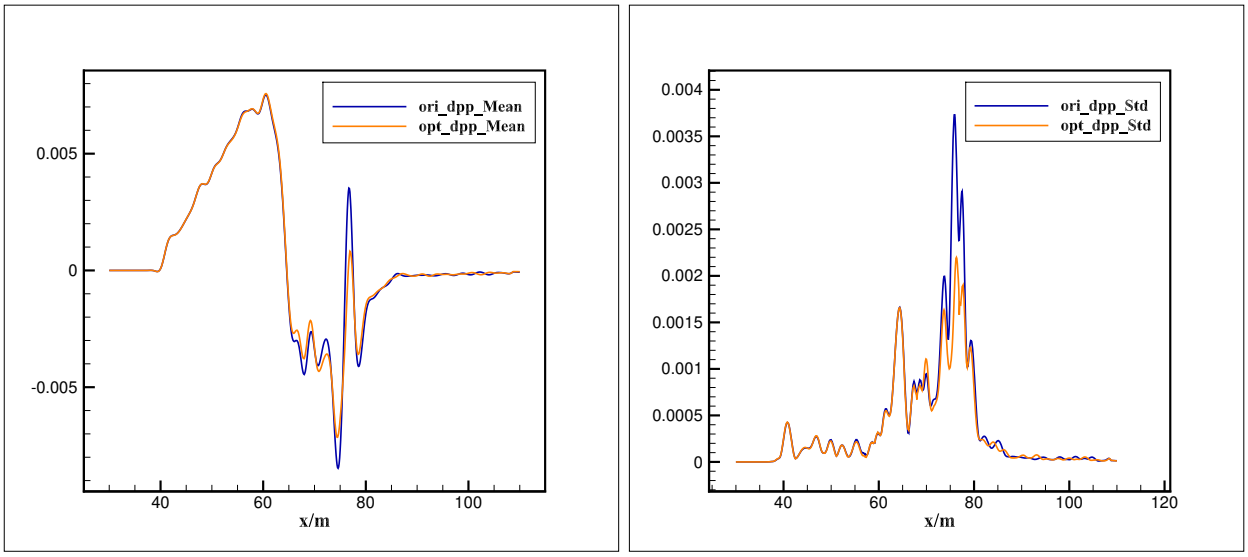


Figure 9 – Streamwise distributions of the mean and standard deviation of near-field pressure perturbations before and after robust optimization.

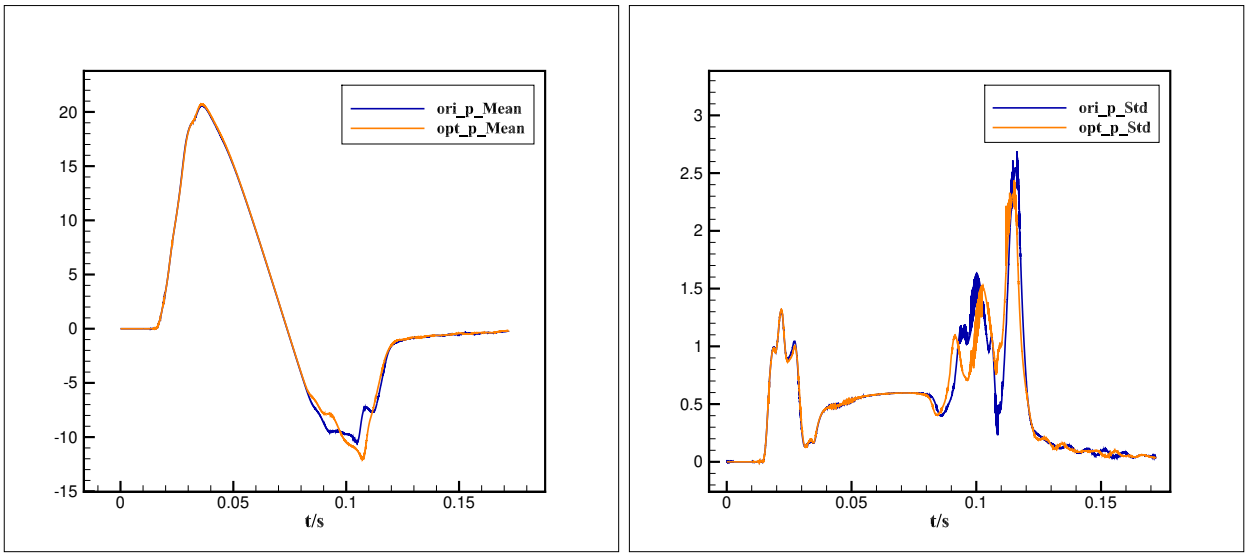


Figure 10 – Temporal distributions of the mean and standard deviation of ground pressure signatures before and after robust optimization.

Table 5 – Mean and standard deviation of C_l, C_d and PLdB for the baseline and optimized configurations.

	Cl		Cd		PLdB	
	mean	std	mean	std	mean	std
Ori	0.07315	0.00261	0.01178	0.00017	83.48035	1.25764
Opt	0.07364	0.00262	0.01176	0.00017	82.37783	0.67727

6. Conclusions

This paper presented a sparse polynomial chaos expansion-based framework for aerodynamic and sonic boom robust optimization under multi-source parametric uncertainty. The framework combines sparse surrogate construction with a statistical optimization formulation so that repeated uncertainty propagation can be performed efficiently in an otherwise expensive high-fidelity design problem.

Application to the JAXA wing-body configuration showed that the proposed approach can preserve the statistical level of aerodynamic performance while achieving a meaningful reduction in both the mean and the standard deviation of the sonic boom loudness metric PLdB. Analysis of the near-field and ground-pressure statistics further indicated that the optimized design reduces both waveform intensity and response variability in the most influential wave-dominated regions.

Overall, the results indicate that sparse PCE is a practical surrogate-modeling strategy for robust aerodynamic and sonic boom design with limited samples. Future work should focus on expanding the present framework to larger design spaces, more detailed atmospheric uncertainty models, and comparative studies against alternative surrogate-assisted robust optimization methods.

7. Contact Author Email Address

Huan Zhao: huanzhao@nwpu.edu.cn

8. Copyright Statement

The authors confirm that they, and/or their company or organization, hold copyright on all of the original material included in this paper. The authors also confirm that they have obtained permission, from the copyright holder of any third party material included in this paper, to publish it as part of their paper. The authors confirm that they give permission, or have obtained permission from the copyright holder of this paper, for the publication and distribution of this paper as part of the ICAS proceedings or as individual off-prints from the proceedings.

9. Acknowledgement

This work was sponsored by the National Natural Science Foundation of China (NSFC) under grant No. 52572420 and the foundation of National Key Laboratory of Aircraft Configuration Design under grant No. JBGS-202502. These supports are gratefully acknowledged.

References

[1] Michael Colonno and Juan Alonso. Sonic Boom Minimization Revisited: The Robustness of Optimal Low-Boom Designs. In *13th AIAA/ISSMO Multidisciplinary Analysis Optimization Conference*, Fort Worth, Texas, September 2010. American Institute of Aeronautics and Astronautics.

[2] Yoshikazu Makino and Ilan Kroo. Robust Objective Functions for Sonic-Boom Minimization. *Journal of Aircraft*, 43(5):1301–1306, September 2006.

[3] Zhao Huan, Gao Zhenghong, Xu Fang, and Zhang Yidian. Review of Robust Aerodynamic Design Optimization for Air Vehicles. *Archives of Computational Methods in Engineering*, 26(3):685–732, July 2019.

[4] Sharon L. Padula, Clyde R. Gumbert, and Wu Li. Aerospace applications of optimization under uncertainty. *Optimization and Engineering*, 7(3):317–328, September 2006.

[5] Thomas K. West, Bryan W. Reuter, Eric L. Walker, Bil Kleb, and Michael A. Park. Uncertainty Quantification and Certification Prediction of Low-Boom Supersonic Aircraft Configurations. *Journal of Aircraft*, 54(1):40–53, January 2017.

[6] Eric Walker, Jeremy T. Pinier, Thomas West, and Kathrine Bretl. Sonic Boom Pressure Signature Uncertainty Calculation and Propagation to Ground Noise (Invited). In *53rd AIAA Aerospace Sciences Meeting*, Kissimmee, Florida, January 2015. American Institute of Aeronautics and Astronautics.

[7] Shinkyu Jeong, Daichi Ono, Koji Shimoyama, and Atsushi Hashimoto. Sonic Boom Analysis under Conditions of Atmospheric Uncertainty Using Polynomial Chaos. *TRANSACTIONS OF THE JAPAN SOCIETY FOR AERONAUTICAL AND SPACE SCIENCES*, 56(3):129–136, 2013.

[8] Huseyin Emre Tekaslan, Sihmehmet Yildiz, Yusuf Demiroglu, and Melike Nikbay. Implementation of Multidisciplinary and Multifidelity Uncertainty Quantification Methods for Sonic Boom Prediction. *Journal of Aircraft*, 60(2):410–422, March 2023.

[9] Sriram K. Rallabhandi, Thomas K. West, and Eric J. Nielsen. Uncertainty Analysis and Robust Design of Low-Boom Concepts Using Atmospheric Adjoints. *Journal of Aircraft*, 54(3):902–917, May 2017.

[10] Jing Li, Zhenghong Gao, Jiangtao Huang, and Ke Zhao. Robust design of NLF airfoils. *Chinese Journal of Aeronautics*, 26(2):309–318, April 2013.

[11] Ke Zhao, Zheng-hong Gao, and Jiang-tao Huang. Robust design of natural laminar flow supercritical airfoil by multi-objective evolution method. *Applied Mathematics and Mechanics*, 35(2):191–202, February 2014.

[12] Andres S. Padron, Juan J. Alonso, and Michael S. Eldred. Multi-fidelity Methods in Aerodynamic Robust Optimization. In *18th AIAA Non-Deterministic Approaches Conference*, San Diego, California, USA, January 2016. American Institute of Aeronautics and Astronautics.

[13] Koji Shimoyama and Akihiro Inoue. Uncertainty Quantification by the Nonintrusive Polynomial Chaos Expansion with an Adjustment Strategy. *AIAA Journal*, 54(10):3107–3116, October 2016.

[14] John A. Schaefer, David S. Lazzara, and Stephen T. LeDoux. Robust Design of Sonic Boom Performance using Spatially Accurate Polynomial Chaos. In *AIAA SCITECH 2023 Forum*, National Harbor, MD & Online, January 2023. American Institute of Aeronautics and Astronautics.

[15] Roland Schobi, Bruno Sudret, and Joe Wiart. POLYNOMIAL-CHAOS-BASED KRIGING. *International Journal for Uncertainty Quantification*, 5(2):171–193, 2015.

[16] Lavi R. Zuhal, Kemas Zakaria, Pramudita Satria Palar, Koji Shimoyama, and Rhea Patricia Liem. Polynomial-Chaos–Kriging with Gradient Information for Surrogate Modeling in Aerodynamic Design. *AIAA Journal*, 59(8):2950–2967, August 2021.

[17] Nora Lüthen, Stefano Marelli, and Bruno Sudret. Sparse Polynomial Chaos Expansions: Literature Survey and Benchmark. *SIAM/ASA Journal on Uncertainty Quantification*, 9(2):593–649, January 2021.

[18] Dongbin Xiu and George Em Karniadakis. The Wiener–Askey Polynomial Chaos for Stochastic Differential Equations. *SIAM Journal on Scientific Computing*, 24(2):619–644, January 2002.

[19] Roger Ghanem and P. D. Spanos. Polynomial Chaos in Stochastic Finite Elements. *Journal of Applied Mechanics*, 57(1):197–202, March 1990.

[20] S. Oladyshkin and W. Nowak. Data-driven uncertainty quantification using the arbitrary polynomial chaos expansion. *Reliability Engineering & System Safety*, 106:179–190, October 2012.

[21] Géraud Blatman and Bruno Sudret. Adaptive sparse polynomial chaos expansion based on least angle regression. *Journal of Computational Physics*, 230(6):2345–2367, March 2011.

[22] Shekun Wang, Huan Zhao, Zhengang Zhang, and Weifeng Zhang. An adaptive weighted lasso regression method for sparse polynomial chaos expansion: Application to multi-source uncertainty quantification. *Reliability Engineering & System Safety*, 275:112832, November 2026.

[23] Bradley Efron, Trevor Hastie, Iain Johnstone, and Robert Tibshirani. Least angle regression. *The Annals of Statistics*, 32(2):407–499, 2004.

[24] S. S. Stevens. Perceived Level of Noise by Mark VII and Decibels (*E*). *The Journal of the Acoustical Society of America*, 51(2B):575–601, February 1972.

[25] P Shepherd and M Sullivan. A Loudness Calculation Procedure Applied to Shaped Sonic Booms. NASA Technical Paper 3134, NASA Langley Research Center, November 1991.

[26] Thomas D. Economon, Francisco Palacios, Sean R. Copeland, Trent W. Lukaczyk, and Juan J. Alonso. SU2: An Open-Source Suite for Multiphysics Simulation and Design. *AIAA Journal*, 54(3):828–846, March 2016.